CHEMISTRY OF MATERIALS
Cite This: Chem. Mater. 2020, 32, 27−37
Methods/Protocols
pubs.acs.org/cm

Tracking the Fluorescence Lifetimes of Cesium Lead Halide Perovskite Nanocrystals During Their Synthesis Using a Fully Automated Optofluidic Platform

Ioannis Lignos,*[,†,§] Richard M. Maceiczyk,[†] Maksym V. Kovalenko,[‡,∥] and Stavros Stavrakis*[,†]

[†]Institute for Chemical and Bioengineering, Department of Chemistry and Applied Biosciences, ETH Zurich, Vladimir-Prelog-Weg 1, 8093, Switzerland

[‡]Laboratory of Inorganic Chemistry, Department of Chemistry and Applied Biosciences, ETH Zurich, Vladimir-Prelog-Weg 1, 8093, Switzerland

[∥]Empa − Swiss Federal Laboratories for Materials Science and Technology, Ueberlandstrass 129, CH-8600 Duebendorf, Switzerland

Supporting Information

ABSTRACT: Semiconductive metal halide perovskites have opened exciting opportunities in a range of optoelectronic applications including solar cells, photodetectors, lasers, and light emitting devices. Recently, all-inorganic cesium lead halide ($CsPbX_3$; X = Cl, Br, I) nanocrystals have become attractive light sources due to their high photoluminescence quantum yields, narrow emission linewidths, and emission color tunable over the entire visible region. Their radiative rates are higher (i.e., luminescence lifetimes shorter) than those of more conventional quantum dots, making perovskite NCs brighter emitters, highly attractive as both classical and quantum light sources. Multiple factors—primarily synthesis parameters and postsynthetic experience—govern the observed radiative lifetime and other optical characteristics. High-throughput experimentation in microfluidic platforms equipped with in-line optical characterization had proven to be highly instrumental for rapid and accurate assessment of optical properties, mainly in a steady-state mode. Thus far, in-line measurement of the radiative lifetimes and hence the proper use of high-throughput experimentation for tailored engineering of radiative rates have been elusive. Herein, we showcase a fully automated optofluidic platform that integrates time-correlated single photon counting measurements in droplet-based flow for the rigorous extraction of fluorescence lifetimes of $CsPbX_3$ nanocrystals. The sensitivity of the experimental setup allows for measurements at a single-droplet level. Such concurrent time-resolved photoluminescence allows mapping the parametric space in a time-efficient manner (∼1000 lifetime measurements in 5 h of operation) and with high reagent economy (200 nL reaction volume per measurement). We elucidated the effects of composition and ratios of judiciously chosen reagents, as well as temperature on the fluorescence lifetimes (5−42 ns). Specifically, the average lifetime as well as the emission spectra of all halide compositions tested was strongly dependent on Pb-to-Cs variations. Accordingly a correlation between the steady-state luminescence amplitude and fluorescence lifetimes was established, thus providing a simple method to differentiate between the photoluminescence quantum yields, concentration effects, and effects due to the nonradiative recombination at the surface traps. Such a microfluidic tool will aid in analyzing the physicochemical and photophysical properties of diverse perovskite nanocrystals and other luminescent materials produced in the liquid-state synthesis.

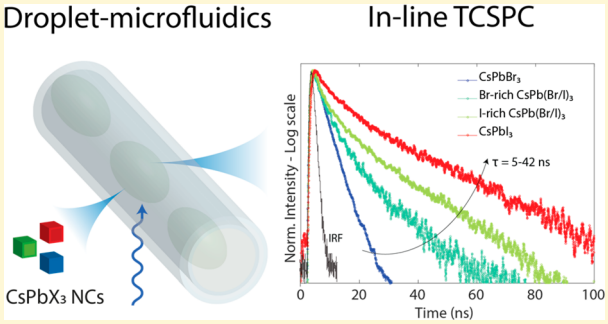

INTRODUCTION

Fluorescence spectroscopy has been paramount as a routine characterization tool in research laboratories focusing on the synthesis and applications of semiconductor nanocrystals (NCs), also known as quantum dots (QDs).[1,2] QDs have been studied intensely due to their unique electronic and optical properties and potential utility in biological luminescent labeling,[3,4] electrically and optically driven light emitting devices,[4−12] photodetectors,[13−16] and photovoltaic devices.[17−23] It is well recognized that reaction parameters during the bottom-up synthesis of QDs (concentrations and molar ratios of precursors and ligands, temperature vs reaction time profile) have a strong influence on the size and morphology of the QDs and the state of the surface, hence drastically altering the photoluminescence quantum yield (PL QY) and other characteristics of the formed particles.[23] In general, measurement of the decay in PL of species after excitation by a short optical pulse allows for the determination of both radiative (k_r)

Received: August 23, 2019
Revised: December 4, 2019
Published: December 9, 2019

DOI: 10.1021/acs.chemmater.9b03438
Chem. Mater. 2020, 32, 27−37

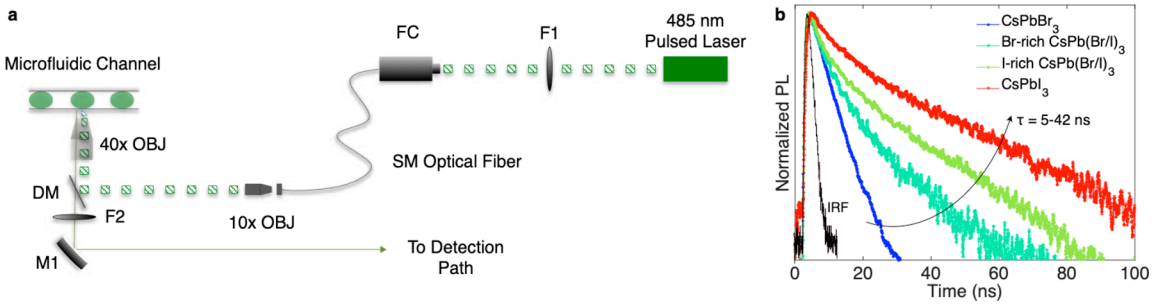

Figure 1. (a) Schematic of the microfluidic platform incorporating a TCSPC module. (b) Representative in situ PL decays of $CsPbX_3$ NCs and the instrument response function (IRF). Radiative lifetimes were estimated using a multiexponential fitting function in real time.

and nonradiative rate (k_{nr}) coefficients, which control and define the PL quantum efficiency.[24] Accordingly, the ability to perform on-the-fly time-correlated single photon counting (TCSPC) measurements, when synthesizing nanoparticles, will significantly enhance useful information content by providing an absolute measure independent of sample concentration. For example, evaluation of PL lifetime components will reveal whether an increase in the time-integrated emission intensity is due to an increase in PL QY (eq 1) or the product concentration, with the latter not causing any change in the average fluorescence lifetime (τ) (eq 2).[24]

$$\text{PL QY} = \frac{k_r}{k_r + k_{nr}} \tag{1}$$

$$\tau = \frac{1}{k_r + k_{nr}} \tag{2}$$

Lead halide perovskite NCs (LHP NCs) are exceptional materials for a range of nanomaterial-based optoelectronic applications, including photonic sources[2,10,25−33] and light harvesters.[19−21,34,35] Numerous synthetic approaches have been reported for the formation of colloidal $APbX_3$ NCs with Cs, formamidinium (FA), and methylammonium (MA) or mixtures thereof as ions of the A-site and various halides.[2,31,34,36−45] In recent years, all-inorganic $CsPbX_3$ NCs have attracted enormous attention due to their near-unity QYs and facile compositional tuning of their emission and absorption energies across the entire visible region of the electromagnetic spectrum.[2] Several methodologies have been reported for the elucidation of their nucleation and growth mechanisms,[46,47] surface chemistry,[48−53] and photophysics.[54−60] However, a detailed understanding of the reaction parameters that govern their physicochemical and photophysical characteristics is limited by the rapid kinetics of nucleation and growth associated with ionic-metathesis-based processes.[2,46] Additionally, the phase instability of the 3D polymorph of $CsPbI_3$ or $CsPb(Br/I)_3$ NCs limits photophysical characterization for certain cationic or halide compositions.[61]

Near-future anticipated applications of LHP NCs are in liquid crystal displays (LCDs)[62] exploiting bright narrow-band PL or in light emitting diode (LED) displays[63] making use of electroluminescence. Beyond these classical applications, information regarding the fluorescence lifetimes of perovskite NCs is significant for the development of quantum light sources, such as single-photon LEDs[64] or for quantum information technologies.[60,65] $CsPbX_3$ NCs have short radiative lifetimes (few nanoseconds at room temperature), typically an order of magnitude faster than InP or CdSe QDs and 3 orders of magnitude faster at cryogenic temperatures, which makes them ideal candidates for the development of single-photon sources.[56,66] Perovskite NCs are thus far the most optically coherent chemically synthesized single-photon sources.[60] An important aspect is that the profile of the PL decay and the average radiative lifetime can be related to NC stability. A recent study by Bodnarchuk et al.[43] exemplifies the effects of surface passivation and aging on PL lifetimes and PL QYs, elucidated by standard ex situ optical measurements. It is therefore a highly desired prerequisite to develop a strategy for the direct in situ and cost-efficient evaluation of the PL lifetimes in response to the synthesis conditions, isolation, and purification steps.

As noted, TCSPC measurements can provide a detailed analysis of excited state dynamics through the evaluation of PL decay time components.[24] That said, NC characterization is normally performed in an off-line manner (for NCs synthesized in flask reactors), using methods based on time-integrated and time-resolved fluorescence, absorption spectroscopy, and light scattering.[67,68] Automation of batch synthetic processes, together with the rapid optimization of the physicochemical and photophysical properties of the resulting NCs, is almost always challenging, due to the need for extensive sample preparation, the difficulties associated with detector integration, and the need for particle purification postsynthesis.[68,69] This is particularly crucial for the discovery and development of more complex perovskite compositions, such as emerging double perovskite NCs, with recent examples being $Cs_2Ag_{1-x}Na_xInCl_6$,[70,71] $Cs_2AgIn_xBi_{1-x}Cl_6$,[72] and Cs_2AgBiX_6.[73] In such systems, PL QY and PL lifetimes are determined by a complex interplay among doping strategies, B-site ions, and reaction conditions, which makes the thorough parametric screening prohibitively slow with conventional flask synthesis and postsynthetic optical characterization. Conversely, microfluidic platforms incorporating optical detection systems have been shown to allow for the controlled synthesis of a wide range of NCs, together with efficient and real-time characterization of material properties.[31,44−46,74−86] In this regard, most efforts have focused on in-line implementations of techniques such as fluorescence and UV−visible absorption,[75,87] X-ray scattering,[88] and correlation spectroscopies,[89] with information regarding particle size, shape, and size distribution being accessible.

Recently, we reported the microfluidic syntheses of $CsPbX_3$, $FAPbX_3$, and $Cs_xFA_{1-x}Pb(Br_{1-y}I_y)_3$ NCs, together with rigorous and ultrafast mapping of reaction parameter space, including molar ratios of cation and halide precursors, ligands, reaction temperatures, and reaction times.[31,44−46,83] The combination of efficient mass/thermal transport and real-

DOI: 10.1021/acs.chemmater.9b03438
Chem. Mater. 2020, 32, 27−37

time product analysis within a versatile microfluidic platform allowed for the investigation of early stage reaction kinetics and provided both optimized and transferable synthesis parameters for conventional flask-based reaction systems. Although highly successful, further refinement of such an approach is required to allow the efficient extraction of real-time information regarding PL QYs and radiative/nonradiative deactivation pathways. To this end, herein we report the implementation of a fully automated optofluidic platform (Figure 1a), which combines both time-integrated and time-resolved PL detection for the comprehensive and systematic investigation of the effect of different reaction parameters, including temperature, I/Br ratios, and Pb/Cs ratios, on the PL lifetime of $CsPbX_3$ NCs. We show for the first time that a correlation between the sample brightness and radiative lifetime can be established, without the need for sample isolation and purification. This innovation allows a simple route to differentiating between the concentration effects and effect due to the nonradiative recombination in surface traps. TCSPC measurements allow for in situ decoding of PL decaytimes (between 5 and 42 ns) for all halide systems studied and highlights critical reaction parameters that have a strong influence on PL QYs. The range of extracted fluorescence decay time components is in line with previous flask-based methodologies,[2] indicating the accuracy and precision of the developed methodology. In particular, in-line TCSPC measurements allow for a further understanding of the photophysical characteristics of $CsPbX_3$ NCs under both Cs-rich (Pb/Cs $\leq$ 1.5) and Pb-rich (Pb/Cs $\leq$ 1.5) synthetic conditions.

EXPERIMENTAL SECTION

Materials. Cesium carbonate (Cs_2CO_3, Aldrich, 99.9%), lead bromide ($PbBr_2$, ABCR, 98%), lead iodide (PbI_2, ABCR, 99.999%), 1-octadecene (ODE, 90%), oleic acid (OA, Sigma-Aldrich, 90%), oleylamine (OLA, Acros, ≥96%), perfluorooctyltrichlorosilane (PFO, Sigma-Aldrich, 97%), fluorescein isothiocyanate (FITC), phosphate-buffered saline (PBS), potassium hydroxide (KOH, Sigma-Aldrich, ≥86%), erythrosine B (Sigma-Aldrich, dye content ≥95%), potassium iodide (KI, Sigma-Aldrich, ≥99%), and Galden perfluoropolyether fluorinated (PFPE) fluid (Blaser Swisslube) were used as received.

Preparation of Precursors. *Cesium Oleate Precursor Solution.* Cs_2CO_3 (0.204 g), ODE (40 mL), and OA (2.5 mL) were placed in a 100 mL Schlenk flask and dried at 120 °C under vacuum for 2 h to allow dissolution of the cesium salt. The solution was then allowed to cool and could then be stored under argon for several days without any observable precipitation at room temperature. For each experiment, 8 mL of precursor solution was loaded into a 10 mL gastight glass syringe (Hamilton).

Lead Halide Precursor Solution. PbX_2 including $PbBr_2$ (0.069 g) and PbI_2 (0.087 g) were added to 20 mL Schlenk flasks together with 5 mL of ODE and dried under vacuum for 2 h at 120 °C. After this period of time, 0.8 mL of dried OA and dried OLA were added under argon until all the PbX_2 is completely dissolved. The resulting solutions were then allowed to cool to ambient before being loaded into 10 mL gastight glass syringes (Hamilton).

Microfluidic Platform and Experimental Procedure. Precision syringe pumps (neMESYS, Cetoni GmbH, Germany) were used to inject and motivate the dispersed phase (i.e., PbX_2 and Cs−oleate precursor solutions) and carrier fluid (Galden perfluoropolyether fluorinated fluid) toward a PEEK cross (P-729, Upchurch Scientific, Germany) to form a segmented flow of droplets. For $CsPb(X/Y)_3$, the dispersed PbX_2 and PbY_2 precursor solutions were initially injected into a PEEK T-junction before being loaded into the PEEK cross for droplet formation. The injection cross and the syringes carrying the precursor solutions were connected through PTFE tubing (ID 250 μm, OD 1/16 in., Upchurch Scientific, Germany) using PEEK fingertight fittings (F-127, Upchurch Scientific, Germany). The carrier fluid was transferred to the PEEK cross through fluorinated ethylene propylene tubing (ID 750 μm, OD 1/16 in., Upchurch Scientific, Germany). Typical flow rates for the carrier phase were between 50 and 120 μL/min and between 0.5 and 30 μL/min for the dispersed phase. As previously reported, the microfluidic platform allowed for independent control of the Pb-to-Cs molar ratio and halide ratios (I-to-Br) through adjustment of flow rate ratios at the cross and T-junctions, respectively. The formed droplets containing the reaction mixture were subsequently directed through perfluoroalkoxy alkane (PFA) tubing (ID 500 μm, OD 1/16 in., Upchurch Scientific, Germany) coiled around a copper-heating rod (diameter = 1.5 cm) to allow the initiation of reaction. Droplets exiting the heating section were directed through PTFE tubing into a straight channel (500 × 80 μm) polydimethylsiloxane (PDMS) microfluidic flow cell to allow for concurrent time-integrated and time-resolved measurements. The PDMS microfluidic device was fabricated using standard soft-lithographic techniques, which are described elsewhere.[90] Surface treatment of the microfluidic channels with PFO was performed prior to each experiment to ensure that channel surfaces were consistently fluorophilic.

Confocal Fluorescence Detection. For all TCSPC experiments, light from a 485 nm pulsed diode laser (LDH P-C-485B, 90 ps pulse width, PicoQuant GmbH, Germany) was directed toward a laser cleanup filter (*F1*) (F49−488, AHF, Germany) and then coupled by a fiber delivery system (*FC*) using a single mode fiber (KineFLEX-P-3-S-488, QIOPTIQ, Germany). Light exiting the fiber was then collimated by an infinity-corrected 10× magnification microscope objective (Olympus 10× NA 0.25, Thorlabs, Germany) for laser beam expansion and directed into the back port of the microscope (Nikon Ti-E, Nikon, Switzerland). Expansion of the laser beam ensured that the beam almost completely fills the entire back aperture of the objective lens (~6.5 mm) and minimizes the laser spot diameter at the focal point. Subsequently, a dichroic mirror (*DM*) (F48-510, AHF, Germany) reflected the light into a 40× air objective (40× Plan Fluor Nikon NA 0.75, Nikon, Switzerland). Fluorescence emission from the sample was collected by the same objective lens and filtered by an emission filter (*F2*) (F76-490:488 LP Edge Basic Longpass Filter, AHF, Germany) which was installed in the microscope filter cube together with the dichroic mirror. A mirror (*M1*) was then used to reflect the fluorescence into the detection path. Fluorescence emission was then focused by the microscope tube lens (*L1*) onto a 30 μm pinhole (*PH*) (P30S Mounted Precision Pinhole, Thorlabs, Germany) to reject out-of-focus photons. A collimating lens (*L2*) (f =100 mm, Thorlabs, Germany) was used to collimate the light, and a holographic notch filter (*NF*) (F40-487: Single Notch Filter for 488 nm - E grade, AHF, Germany) used to remove residual back-reflected excitation light, before the fluorescence was directed onto a continuously variable neutral density filter wheel (*FW*) (Cage-Compatible,

DOI: 10.1021/acs.chemmater.9b03438
Chem. Mater. 2020, 32, 27−37

Cont. Variable, Refl. ND Filter Wheel, OD = 0−2.0, M4 Tap, Thorlabs, Germany). Finally, fluorescence was focused by a lens (*L3*) and directed onto a SPAD photodetector (SPCM-AQRH 13, Excelitas, Canada). The system integrates compact TSCPC electronics, allowing for PL lifetime measurements with a temporal resolution of 25 ps. Briefly, the TCSPC electronics are based on a TimeHarp 260 stand-alone module (PicoQuant GmbH, Germany). This system can record digital photon detection signals in time-tagged, time-resolved (TTTR) mode, allowing the delay time of each fluorescence photon with respect to the laser pulse to be recorded.

In Situ PL Measurements and Estimation of Fluorescence Lifetimes. In situ PL intensity and lifetime measurements of $CsPb(X/Y)_3$ NCs were recorded from individual droplets traveling along the PDMS microfluidic channel. PL data were recorded with a 100 ms integration time using a fiber spectrometer (Qe Pro, Ocean Optics, U.K.) through a 2 m long fiber mounted to one of the ports of the microscope. TCSPC measurements were recorded with a 50−100 ms integration time, 0.025 ns binning time, and 10 s total acquisition time, by further averaging over multiple droplets. In-house software (written in the LabView programming environment) was used to calculate real-time fluorescence decay times of the synthesized NCs, with decay profiles being fitted to a sum-of-exponential models containing up to three terms, eq 3. The fluorescence decay measured by the TCSPC method corresponds to the convolution of the instrument response function (IRF) of the microscope with the actual fluorescence decay of the sample. Since the IRF affects the accuracy of measured fluorescence lifetime, we measure its value by an IRF deconvolution procedure to improve the accuracy of the lifetime measurement. The solution for the IRF measurement was prepared by the mixing 170 μL of saturated Erythrosine B solution with 300 μL of 0.004 M KOH solution in 1 mL of water solution containing saturated KI.

$$I(t) = I_0 \sum_{i=1}^{n} \exp\left(\frac{t}{\tau_i}\right) \tag{3}$$

Here $I(t)$ is intensity at time t, I_0 is the intensity at time zero, and τ_i is the lifetime of the ith component. The average lifetime (τ) was calculated using eq 4, with parameter estimation being performed in an iterative fashion by minimization of the reduced chi-squared parameter, i.e.,

$$\tau = \frac{\sum_{i=1}^{n}(a_i\tau_i^2)}{\sum_{i=1}^{n}(a_i\tau_i)} \sum a_i = 1 \tag{4}$$

Here, a_i is the amplitude (or pre-exponential factor) associated with component i, where $\sum a_i = 1$. A Levenberg−Marquardt minimization algorithm was used to fit all data, and a Richardson−Lucy algorithm was used for the deconvolution of the IRF from recorded decay profiles. The analysis software allows control of the number of fitting parameters, with the initial parameter estimates being provided manually at the start the fitting procedure. Fitting of the fluorescence decays originating from the synthesized NCs (within individual droplets) can be performed in high-throughput, with the average fluorescence lifetime being calculated in an automatic manner (see Figure S1 for single droplet fluorescence lifetime analysis).

It is important to note that the reactor operation is entirely automated and is also controlled by a custom-made LabView script. Briefly, the LabView script accepts a set of predefined experimental parameters that are executed in sequence. First, the reactor checks current reaction conditions (such as temperature and volumetric flow rates) and then determines an appropriate time scale for the system to reach steady-state. Reaction conditions are then adjusted, and after measurement of fluorescence decay curves, fluorescence decay times are extracted. Figure 2 summarizes the workflow for this process.

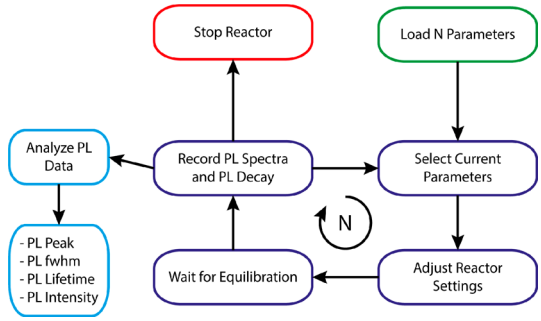

Figure 2. Flowchart for the automated operation of the microfluidic platform and recording of PL lifetimes and PL spectra.

RESULTS AND DISCUSSION

To calibrate the real-time TCSPC detection system and assess the robustness of the analysis procedure, we measured the fluorescence decay of a 100 μM fluorescein isothiocyanate (FITC) solution in PBS buffer enclosed in nanoliter droplets. The fluorescence decay profile is shown in Figure 3 and is satisfactorily described by a single exponential decay function with a fluorescence lifetime of 4.18 ns and a reduced chi-squared value of 1.23.

Colloidal $CsPbX_3$ NCs were then synthesized according to procedures described in our recent publication.[46] As previously elucidated, the molar ratio of Pb-to-Cs should be maintained above 1.5 to ensure that the synthesis can proceed in the stoichiometric fashion with full reaction yield (forming Pb−oleate as a byproduct).[46] In particular, multiple variations of Pb-to-Cs reagent ratios can have a dramatic effect on PL properties, such as fwhm and PL intensity. Additionally, Pb-rich conditions (Pb-to-Cs molar ratios between 2 and 5, depending on the halide composition) can be beneficial for the formation of $CsPbX_3$ NCs with enhanced PL QYs.[46] To further understand the effect of the particle concentration on time-integrated fluorescence intensities and to develop a better understanding of the decay dynamics of $CsPbBr_3$, $CsPb(Br/I)_3$, and $CsPbI_3$ NCs, we primarily focused our studies on the impact of Cs and Pb loadings on the fluorescence decays, the associated radiative lifetimes, and the PL intensities.

Figure 4a illustrates variations in the time-integrated PL emission spectra as a function of the Pb-to-Cs molar ratio, with Figure 4b presenting corresponding fluorescence decay profiles for the same conditions. More specifically, changes in PL intensity recorded in-line for Br-rich $CsPb(Br/I)_3$ NCs (iodide loading is equal to 16% based on the halide flow-rate ratios) results in variations of their fluorescence lifetime. The PL decay spectra can be fitted by a biexponential function providing in real time the (τ_1) and (τ_2) components, whereas the average recombination lifetime is estimated by eq 4. The non-monoexponential decay profile is also in line with the trend observed for $CsPbBr_3$ NCs.[43] A formidable challenge

DOI: 10.1021/acs.chemmater.9b03438
Chem. Mater. 2020, 32, 27−37

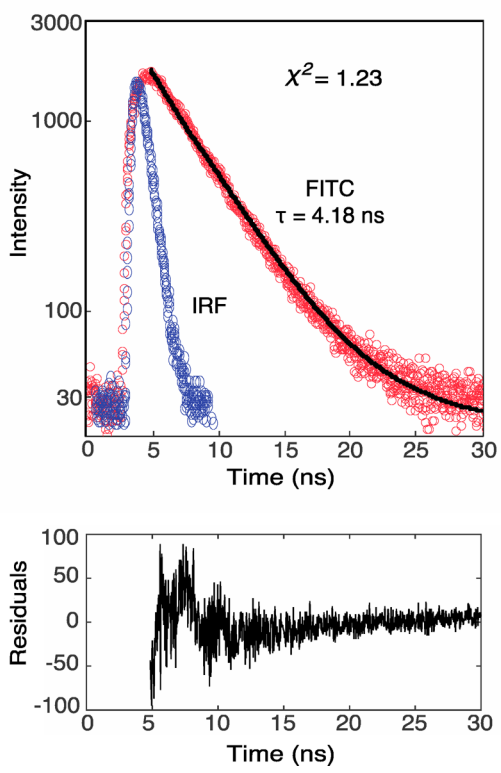

Figure 3. Fluorescence lifetime analysis of a 100 μM FITC solution in PBS buffer. Other parameters were λ_{ex} = 488 nm, pulse width = 80 ps, and repetition rate = 20 MHz.

with perovskite NCs is to relate monoexponential decays (typically higher QYs) and multiexponential decays (typically lower QYs) with PL QY.[43] Typically, surface traps usually shorten the measured PL lifetime due to fast, irreversible nonradiative trapping of one of the photoexcited carriers. However, shallow trap states may only temporally trap the carrier and eventually return, yielding a long-lived component to the PL.[91−93]

For instance, Figure 4c illustrates that an increase of the Pb-to-Cs molar ratio from 1.7 to 3.1 leads to an increase of the average fluorescence lifetime from 17.2 to 19.2 ns, whereas a further increase of Pb-to-Cs ratio causes a drop to 13.5 ns probably associated with the nonradiative recombination. The average lifetime of all halide compositions tested has a strong dependence on Pb-to-Cs variations (see Supporting Information for additional studies of Pb-to-Cs variations at different temperatures, Figures S2−S4), particularly for $CsPbI_3$ where the average lifetime drops from 44 to 15 ns for Pb-rich NCs.

To obtain additional insights into the role of NC compositional changes on the PL properties, we also measured the fluorescence lifetimes of $CsPb(Br/I)_3$ NCs while varying the halide composition. As shown in our recent study,[46] the band edge emission of Br/I perovskites can be tuned from 523 to 690 nm through a continuous variation of $PbI_2/PbBr_2$ halide molar ratio (Supporting Information for PL spectra). In general, PL lifetime is both composition and size-dependent at room temperature. Specifically, for larger bandgaps—smaller NC sizes or lighter halides—the PL lifetime is shorter.[55] Such bandgap dependence of the radiative rate is fully explainable by the Fermi golden rule, also known as the energy gap law.[94] In this direction, adjustment of the anionic composition of the synthesized $CsPbX_3$ NCs serves two purposes: it provides a facile manner to tune the PL properties of the perovskite NCs, and at the same time possible size-dependent effects on the measured PL lifetimes can be excluded when the size of $CsPbX_3$-based NCs is fixed between 10 and 12 nm (e.g., within the weak quantum confinement regime).[59,66] Figure 5a,b demonstrates the effect of the halide content on the normalized fluorescence decays of $CsPb(Br/I)_3$ NCs. Extractions of the average fluorescence lifetimes from the fluorescence decay data were plotted as a function of iodide content and showed a practically linear increase.

Previously, we demonstrated that the band edge emission and the PL decays of $CsPb(Br/I)_3$ can be tuned as a function of I/Br molar ratio.[46] Therefore, by a systematic variation of iodide loading from 6.5 to 91.6%, we managed to tune the PL peak wavelength from 516 to 680 nm (Figure 5c) leading to a monotonic increase of average PL lifetimes from 12.5 (Br-rich) to 30 ns (I-rich) (Figure 5b). This confirms that the PL lifetime is strongly dependent on the halide confirming that the heavier the halide, the longer the PL lifetime. However, the long PL lifetime could also be attributed to the formation of metastable charge-separated states involving electrons in shallow surface traps.[91]

To further investigate the effect of iodide content on the fluorescence decays, we conducted experiments at various temperatures with a fixed Pb-to-Cs molar ratio. Figure 5d demonstrates the effect of iodide loading from 6.5 to 91.6% on the average lifetime of the synthesized NCs, at 150, 170, and 180 °C (temperatures correspond to the synthesis of NCs—

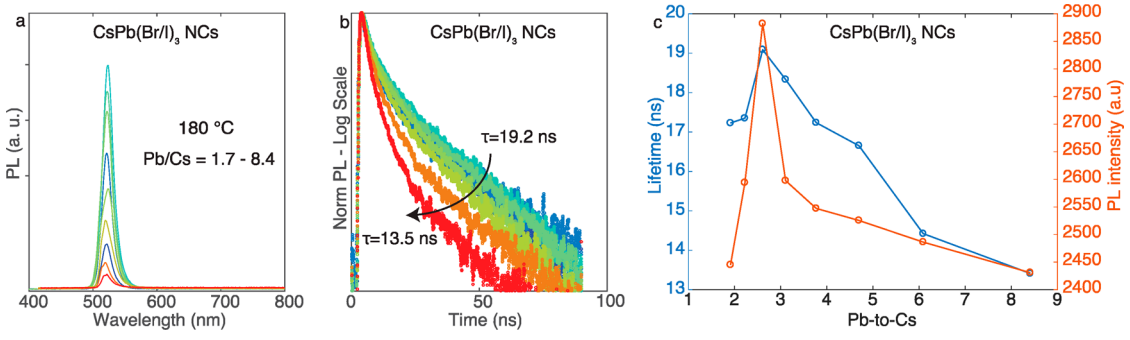

Figure 4. Effect of the Pb-to-Cs molar ratio on the (a) PL characteristics and (b) normalized fluorescence decays (log-scale) of $CsPb(Br/I)_3$ NCs at 180 °C. Colors in the PL spectra correspond to various Pb/Cs values. The PL decays were fitted using a biexponential model, and they are extracted after averaging over multiple droplets with the same experimental conditions. (c) Pb-to-Cs molar ratios vs τ and PL intensity for the synthesized $CsPb(Br/I)_3$ NCs. Other reaction conditions were fixed to reaction time = 10 s and iodide loading = 16%.

DOI: 10.1021/acs.chemmater.9b03438
Chem. Mater. 2020, 32, 27−37

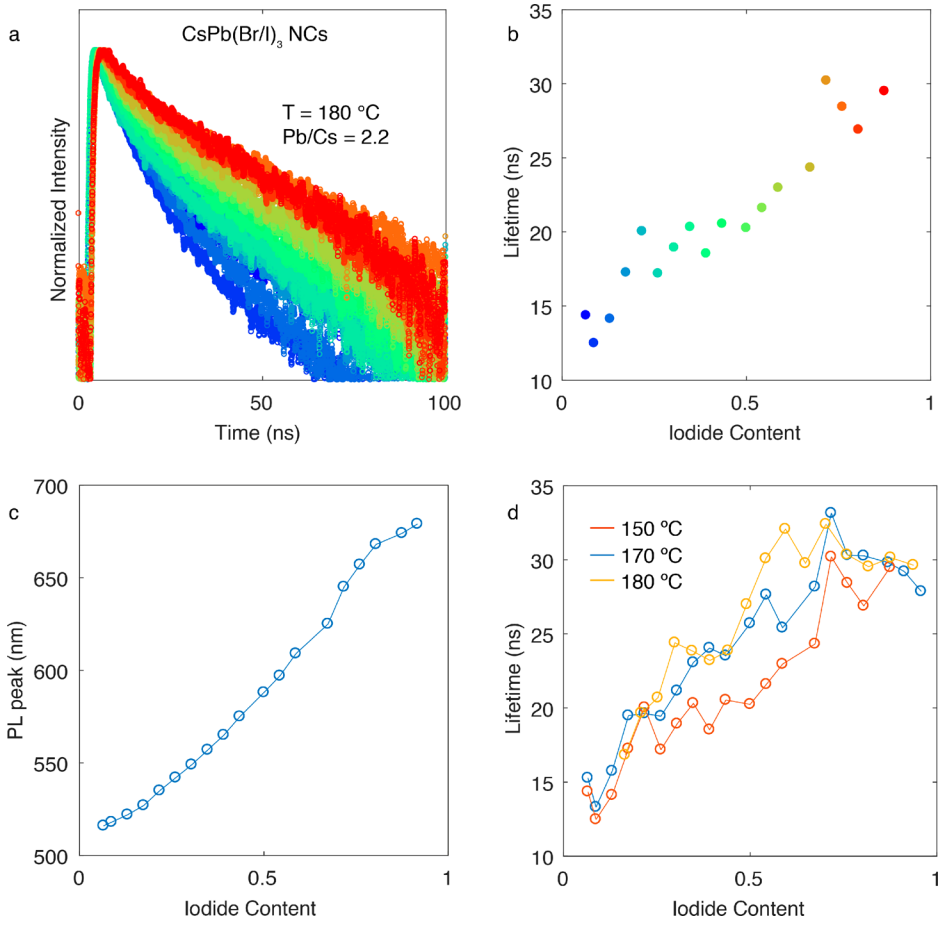

Figure 5. Effect of iodide loading on the (a) normalized fluorescence decays (log-scale), (b) average lifetimes (τ), and (c) position of maximum emission of $CsPb(Br/I)_3$ NCs at 170 °C. Colors in Figure 5b correspond to the fluorescence decays in Figure 5a. The PL decays were fitted using a biexponential model, and they are extracted after averaging over multiple droplets with the same experimental conditions. (d) Iodide content vs average lifetime for $CsPb(Br/I)_3$ NCs which were synthesized at various temperatures of 150, 170, and 180 °C. Other reaction conditions were fixed to Pb-to-Cs = 2.2 and reaction time = 10 s.

lifetime measurements were conducted at room temperature, after droplets exiting the reactor). Although fluorescence lifetimes tend to increase at all temperatures, at iodide loadings between 25 and 50% they remain mostly constant or slightly decrease. This can be explained by the fact that at this range of iodide loading a drop in PL intensity is observed, mostly due to the fast halide-ion segregation during the formation of $CsPb(Br/I)_3$ NCs.[61]

Although variation of the anionic composition toward the formation of Br-rich and I-rich perovskite NCs provides a facile tuning of their PL spectra from blue to red, a concurrent readjustment of Pb-to-Cs molar needs to be considered.[46] For this reason, we performed experiments at different Pb-to-Cs molar ratios (which has a strong influence on fwhm and emission intensity of $CsPb(Br/I)_3$ while altering the anionic composition of the NCs (see Supporting Information, Figures S5 and S6). In general, Pb-to-Cs molar ratios in the range of 2.2−3.1 allowed for the tuning of the PL lifetimes between 12 and 32 ns from Br-rich to I-rich compositions (Figure 5 and Figure S5). On the other hand, Pb-to-Cs molar ratios greater than 4 do not favor the formation of luminescent Br-rich mixed halide NCs, since the fluorescence lifetime decays of NCs with iodide compositions ≤ 50% could not be detected (see Figure S6, Pb-to-Cs = 4.1). At the same time, average lifetimes of I-rich NCs were considerably lower than those synthesized at lower Pb-to-Cs molar ratios. These findings further support our previous study of different optimized Pb-to-Cs molar ratios for the formation of highly luminescent Br-rich and I-rich $CsPb(Br/I)_3$ NCs.[46]

Typical flask syntheses of $CsPbX_3$ NCs are conducted between 160 and 180 °C for obtaining sizes in the range of 8−12 nm.[2] As it has been reported,[2] an optimum range of reaction temperatures for the synthesis of $CsPbX_3$ NCs, which exhibit high QYs (up to 90%) and narrow emission linewidths, is between 130 and 200 °C. In this respect, such high QYs are relatively uncommon for NCs when synthesized at relatively low temperatures. To extend the optical characterization of $CsPbX_3$ NCs, we investigated the fluorescence lifetime behavior of $CsPbX_3$ NCs as a function of temperature for reaction times of at least 10 s. Figure 6a,b shows the evolution of PL decays and variation of PL lifetimes of halide $CsPbBr_3$ NCs as a function of the synthesis temperature between 150 and 200 °C. The average fluorescence lifetimes (PL decays were fitted with a biexponential model at all temperatures) increase from 7.1 to 11.6 ns due to the quantum confinement effect, where normally red-shifted PL spectra would lead to an increase in the fluorescence lifetime. Further increase of temperature leads to a decrease of fluorescence decay time since typically low PL intensities exist at temperatures higher than 200 °C (see Figure S7 for the corresponding change on

DOI: 10.1021/acs.chemmater.9b03438
Chem. Mater. 2020, 32, 27−37

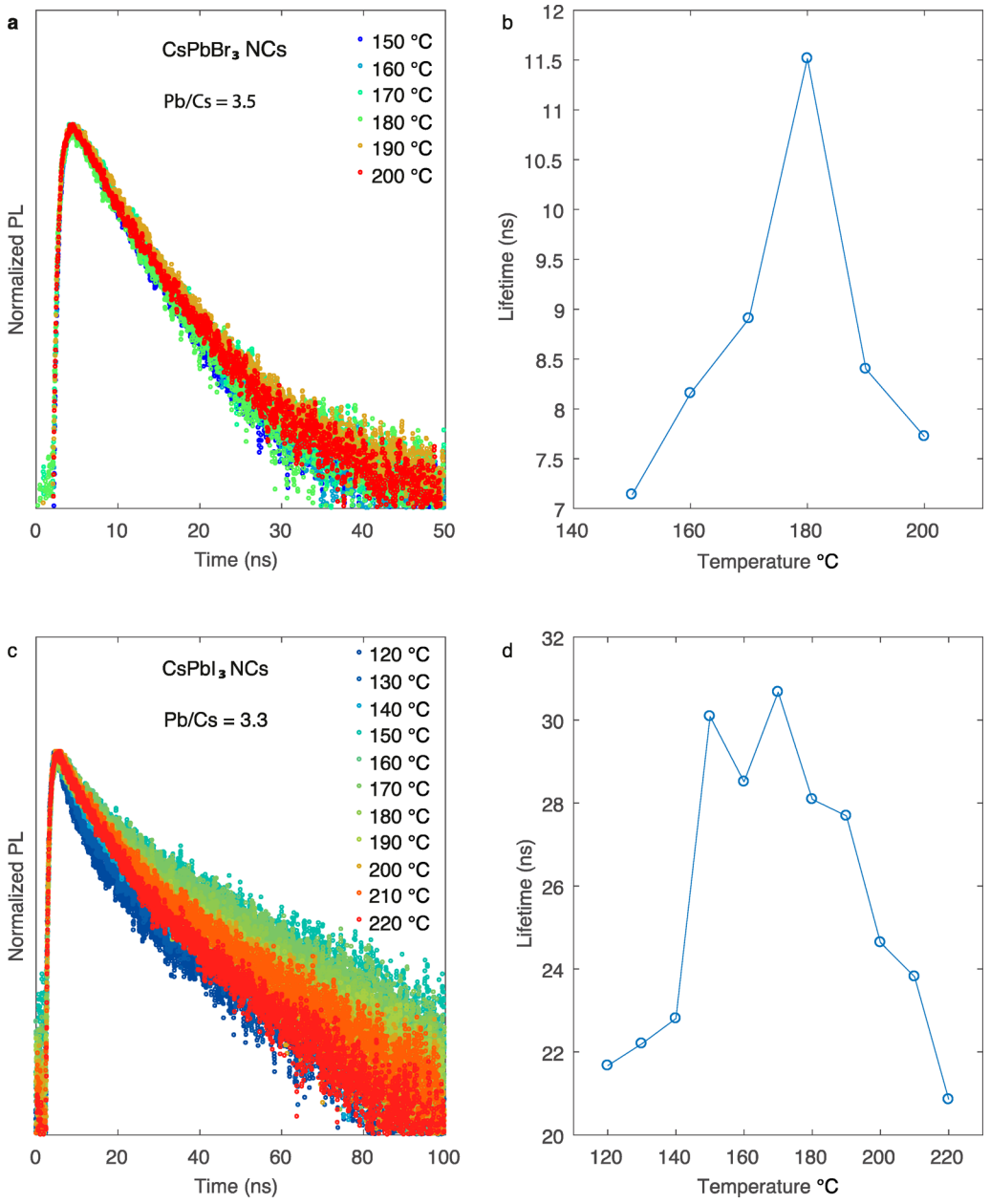

Figure 6. Effect of temperature on the (a, c) normalized fluorescence decays (log-scale) and (b, d) average lifetimes (τ) of $CsPbBr_3$ and $CsPbI_3$ NCs. The PL decays were fitted using a biexponential model, and they are extracted after averaging over multiple droplets with the same experimental conditions. Other reaction conditions were fixed to Pb-to-Cs = 3.5 for $CsPbBr_3$ NCs, Pb-to-Cs = 3.3 for $CsPbI_3$ NCs, and reaction time = 10 s.

PL intensities). A similar behavior is also apparent on Figure 6c,d for the effect of temperature on PL decays and PL lifetimes of $CsPbI_3$ NCs. The same experiments were also conducted for mixed halide perovskite NCs (see Figure S8) revealing a similar behavior for Br-rich and I-rich NCs.

CONCLUSION

The studies described represent the very first report of on-the-fly TCSPC measurements during the synthesis of perovskite NCs and suggest significant potential for the rapid optimization of NC photophysics using minimal reagent volumes (10^6-fold reduction in sample volume compared to conventional analysis) and reduced screening times (~200 experimental runs per hour meaning 100-fold reduction in terms of screening times). In addition, concurrent time-integrated PL and TCSPC measurements revealed that intensity variations from PL measurements were not an effect of product yield but directly proportional to average lifetime. In addition, a thorough investigation on the influence of different precursors (Pb-to-Cs and Br/I ratios) and temperature on the average lifetimes allowed us to verify our conclusions regarding the optimized ratios required for the synthesis of highly luminescent $CsPbX_3$ NCs. In particular, systematic variation of reaction conditions allowed a fine-tuning of the average lifetime between 5 and 42 ns. Importantly, the average lifetime is strongly dependent on the halide content. An increase in the iodide content, for mixed halide perovskites, allowed for a linear increase of the fluorescence lifetimes. However, long PL lifetimes could be attributed to the formation of metastable charge-separated

DOI: 10.1021/acs.chemmater.9b03438
Chem. Mater. 2020, 32, 27−37

states involving electrons in shallow surface traps or polarons. In addition, such platforms are ideally suited for the rapid determination of radiative multinary compositions (such as $CuZnIn(Se/S)_4$ and $Cu(Ga/In)(S/Se)_4$) while providing mechanistic insights based on intrinsic photophysical properties. A refined version of this platform can potentially track the lifetimes of NCs at the early stages of their formation. Elucidating the nucleation and growth mechanism of semiconductor nanocrystals in the millisecond time scale remains challenging. Droplet-based microfluidics integrated with fluorescence lifetime measurements will allow extraction of fluorescence decay times and spectra at early time points during the nucleation growth processes. Experiments toward this goal are in progress. Other applications include protein screening for the extraction of a wide range of parameters (including pH, temperature, and thermodynamics) and fluorescence lifetime-activated droplet sorting. We anticipate that the core methodology will be of immense value to the nanomaterials and microfluidic communities.

■ ASSOCIATED CONTENT

Supporting Information

The Supporting Information is available free of charge at https://pubs.acs.org/doi/10.1021/acs.chemmater.9b03438.

Software snapshot of fluorescence lifetime analysis, the effect of Pb-to-Cs molar ratio on the fluorescence lifetimes of $CsPbI_3$ and $CsPbBr_3$ NCs at various temperatures, the effect of iodide loading on the fluorescence lifetimes of $CsPb(Br/I)_3$ NCs at different Pb-to-Cs molar ratios, and the effect of temperature on PL intensity and average lifetimes of $CsPbBr_3$ and $CsPb(Br/I)_3$ NCs (PDF)

■ AUTHOR INFORMATION

Corresponding Authors

*(I.L.) E-mail: ilignos@mit.edu.

*(S.S.) E-mail: stavros.stavrakis@chem.ethz.ch.

ORCID

Ioannis Lignos: 0000-0002-6816-3290

Richard M. Maceiczyk: 0000-0001-5735-2689

Maksym V. Kovalenko: 0000-0002-6396-8938

Stavros Stavrakis: 0000-0002-0888-5953

Present Address

§(I.L.) Department of Chemical Engineering, Massachusetts Institute of Technology, 77 Massachusetts Avenue, Cambridge, MA 02139, U.S.A

Author Contributions

The manuscript was written through contributions of all authors. All authors have given approval to the final version of the manuscript.

Notes

The authors declare no competing financial interest.

■ ACKNOWLEDGMENTS

The authors would like to thank Dr. Gabriele Raino, Dr. Hendrik Utzat, and Dr. Brent Koscher for discussions and recommendations. This work was partially supported by the Swiss Federal Institute of Technology (ETH Zürich) and by a Swiss National Science Foundation Grant 200021_143638. I. L. was also supported by a Swiss National Science Foundation Grant P2EZP2_172127.

■ REFERENCES

(1) Pietryga, J. M.; Park, Y.-S.; Lim, J.; Fidler, A. F.; Bae, W. K.; Brovelli, S.; Klimov, V. I. Spectroscopic and Device Aspects of Nanocrystal Quantum Dots. *Chem. Rev.* **2016**, *116* (18), 10513−10622.

(2) Protesescu, L.; Yakunin, S.; Bodnarchuk, M. I.; Krieg, F.; Caputo, R.; Hendon, C. H.; Yang, R. X.; Walsh, A.; Kovalenko, M. V. Nanocrystals of Cesium Lead Halide Perovskites (CsPbX3, X = Cl, Br, and I): Novel Optoelectronic Materials Showing Bright Emission with Wide Color Gamut. *Nano Lett.* **2015**, *15* (6), 3692−3696.

(3) Howes, P. D.; Chandrawati, R.; Stevens, M. M. Colloidal nanoparticles as advanced biological sensors. *Science* **2014**, *346* (6205), 1247390−1247390.

(4) Frecker, T.; Bailey, D.; Arzeta-Ferrer, X.; McBride, J.; Rosenthal, S. J. Review - Quantum Dots and Their Application in Lighting, Displays, and Biology. *ECS J. Solid State Sci. Technol.* **2016**, *5* (1), R3019−R3031.

(5) Wood, V.; Bulović, V. Colloidal quantum dot light-emitting devices. *Nano Rev.* **2010**, *1*, 5202−5202.

(6) Chiba, T.; Hoshi, K.; Pu, Y. J.; Takeda, Y.; Hayashi, Y.; Ohisa, S.; Kawata, S.; Kido, J. High-Efficiency Perovskite Quantum-Dot Light-Emitting Devices by Effective Washing Process and Interfacial Energy Level Alignment. *ACS Appl. Mater. Interfaces* **2017**, *9* (21), 18054−18060.

(7) Deng, W.; Xu, X. Z.; Zhang, X. J.; Zhang, Y. D.; Jin, X. C.; Wang, L.; Lee, S. T.; Jie, J. S. Organometal Halide Perovskite Quantum Dot Light-Emitting Diodes. *Adv. Funct. Mater.* **2016**, *26* (26), 4797−4802.

(8) Li, G. R.; Rivarola, F. W. R.; Davis, N. J. L. K.; Bai, S.; Jellicoe, T. C.; de la Pena, F.; Hou, S. C.; Ducati, C.; Gao, F.; Friend, R. H.; Greenham, N. C.; Tan, Z. K. Highly Efficient Perovskite Nanocrystal Light-Emitting Diodes Enabled by a Universal Crosslinking Method. *Adv. Mater.* **2016**, *28* (18), 3528−3534.

(9) Li, J. H.; Xu, L. M.; Wang, T.; Song, J. Z.; Chen, J. W.; Xue, J.; Dong, Y. H.; Cai, B.; Shan, Q. S.; Han, B. N.; Zeng, H. B. 50-Fold EQE Improvement up to 6.27% of Solution-Processed All-Inorganic Perovskite CsPbBr3 QLEDs via Surface Ligand Density Control. *Adv. Mater.* **2017**, *29* (5), 1603885.

(10) Pan, J.; Quan, L. N.; Zhao, Y.; Peng, W.; Murali, B.; Sarmah, S. P.; Yuan, M.; Sinatra, L.; Alyami, N. M.; Liu, J.; Yassitepe, E.; Yang, Z.; Voznyy, O.; Comin, R.; Hedhili, M. N.; Mohammed, O. F.; Lu, Z. H.; Kim, D. H.; Sargent, E. H.; Bakr, O. M. Highly Efficient Perovskite-Quantum-Dot Light-Emitting Diodes by Surface Engineering. *Adv. Mater.* **2016**, *28* (39), 8718−8725.

(11) Tan, Y. S.; Zou, Y. T.; Wu, L. Z.; Huang, Q.; Yang, D.; Chen, M.; Ban, M. Y.; Wu, C.; Wu, T.; Bai, S.; Song, T.; Zhang, Q.; Sun, B. Q. Highly Luminescent and Stable Perovskite Nanocrystals with Octylphosphonic Acid as a Ligand for Efficient Light-Emitting Diodes. *ACS Appl. Mater. Interfaces* **2018**, *10* (4), 3784−3792.

(12) Zhang, X. Y.; Sun, C.; Zhang, Y.; Wu, H.; Ji, C. Y.; Chuai, Y. H.; Wang, P.; Wen, S. P.; Zhang, C. F.; Yu, W. W. Bright Perovskite Nanocrystal Films for Efficient Light-Emitting Devices. *J. Phys. Chem. Lett.* **2016**, *7* (22), 4602−4610.

(13) Konstantatos, G.; Sargent, E. H. Nanostructured materials for photon detection. *Nat. Nanotechnol.* **2010**, *5* (6), 391−400.

(14) Tang, X.; Ackerman, M. M.; Chen, M. L.; Guyot-Sionnest, P. Dual-band infrared imaging using stacked colloidal quantum dot photodiodes. *Nat. Photonics* **2019**, *13* (4), 277−282.

(15) Ramasamy, P.; Lim, D. H.; Kim, B.; Lee, S. H.; Lee, M. S.; Lee, J. S. All-inorganic cesium lead halide perovskite nanocrystals for photodetector applications. *Chem. Commun.* **2016**, *52* (10), 2067−2070.

(16) Gong, M. G.; Sakidja, R.; Goul, R.; Ewing, D.; Casper, M.; Stramel, A.; Elliot, A.; Wu, J. Z. High-Performance All-Inorganic CsPbCl3 Perovskite Nanocrystal Photodetectors with Superior Stability. *ACS Nano* **2019**, *13* (2), 1772−1783.

(17) Kovalenko, M. V. Opportunities and challenges for quantum dot photovoltaics. *Nat. Nanotechnol.* **2015**, *10* (12), 994−997.

(18) Wang, X. H.; Koleilat, G. I.; Tang, J.; Liu, H.; Kramer, I. J.; Debnath, R.; Brzozowski, L.; Barkhouse, D. A. R.; Levina, L.;

DOI: 10.1021/acs.chemmater.9b03438
Chem. Mater. 2020, 32, 27−37

Hoogland, S.; Sargent, E. H. Tandem colloidal quantum dot solar cells employing a graded recombination layer. *Nat. Photonics* **2011**, *5* (8), 480−484.
(19) Sanehira, E. M.; Marshall, A. R.; Christians, J. A.; Harvey, S. P.; Ciesielski, P. N.; Wheeler, L. M.; Schulz, P.; Lin, L. Y.; Beard, M. C.; Luther, J. M. Enhanced mobility CsPbI3 quantum dot arrays for record-efficiency, high-voltage photovoltaic cells. *Sci. Adv.* **2017**, *3* (10), No. eaao4204.
(20) Swarnkar, A.; Marshall, A. R.; Sanehira, E. M.; Chernomordik, B. D.; Moore, D. T.; Christians, J. A.; Chakrabarti, T.; Luther, J. M. Quantum dot-induced phase stabilization of alpha-CsPbI3 perovskite for high-efficiency photovoltaics. *Science* **2016**, *354* (6308), 92−95.
(21) Wheeler, L. M.; Sanehira, E. M.; Marshall, A. R.; Schulz, P.; Suri, M.; Anderson, N. C.; Christians, J. A.; Nordlund, D.; Sokaras, D.; Kroll, T.; Harvey, S. P.; Berry, J. J.; Lin, L. Y.; Luther, J. M. Targeted Ligand-Exchange Chemistry on Cesium Lead Halide Perovskite Quantum Dots for High-Efficiency Photovoltaics. *J. Am. Chem. Soc.* **2018**, *140* (33), 10504−10513.
(22) Kagan, C. R.; Lifshitz, E.; Sargent, E. H.; Talapin, D. V. Building devices from colloidal quantum dots. *Science* **2016**, *353* (6302), aac5523.
(23) Kovalenko, M. V.; Manna, L.; Cabot, A.; Hens, Z.; Talapin, D. V.; Kagan, C. R.; Klimov, V. I.; Rogach, A. L.; Reiss, P.; Milliron, D. J.; Guyot-Sionnnest, P.; Konstantatos, G.; Parak, W. J.; Hyeon, T.; Korgel, B. A.; Murray, C. B.; Heiss, W. Prospects of nanoscience with nanocrystals. *ACS Nano* **2015**, *9* (2), 1012−1057.
(24) Lakowicz, J. R. *Principles of fluorescence spectroscopy*, 3rd ed.; Springer: New York, 2006.
(25) Sutherland, B. R.; Sargent, E. H. Perovskite photonic sources. *Nat. Photonics* **2016**, *10* (5), 295−302.
(26) Kovalenko, M. V.; Protesescu, L.; Bodnarchuk, M. I. Properties and potential optoelectronic applications of lead halide perovskite nanocrystals. *Science* **2017**, *358* (6364), 745−750.
(27) Akkerman, Q. A.; Raino, G.; Kovalenko, M. V.; Manna, L. Genesis, challenges and opportunities for colloidal lead halide perovskite nanocrystals. *Nat. Mater.* **2018**, *17* (5), 394−405.
(28) Song, J. Z.; Li, J. H.; Li, X. M.; Xu, L. M.; Dong, Y. H.; Zeng, H. B. Quantum Dot Light-Emitting Diodes Based on Inorganic Perovskite Cesium Lead Halides (CsPbX3). *Adv. Mater.* **2015**, *27* (44), 7162−7167.
(29) Li, X. M.; Wu, Y.; Zhang, S. L.; Cai, B.; Gu, Y.; Song, J. Z.; Zeng, H. B. CsPbX3 Quantum Dots for Lighting and Displays: Room-Temperature Synthesis, Photoluminescence Superiorities, Underlying Origins and White Light-Emitting Diodes. *Adv. Funct. Mater.* **2016**, *26* (15), 2435−2445.
(30) Huang, H.; Polavarapu, L.; Sichert, J. A.; Susha, A. S.; Urban, A. S.; Rogach, A. L. Colloidal lead halide perovskite nanocrystals: synthesis, optical properties and applications. *NPG Asia Mater.* **2016**, *8*, No. e328.
(31) Lignos, I.; Morad, V.; Shynkarenko, Y.; Bernasconi, C.; Maceiczyk, R. M.; Protesescu, L.; Bertolotti, F.; Kumar, S.; Ochsenbein, S. T.; Masciocchi, N.; Guagliardi, A.; Shih, C. J.; Bodnarchuk, M. I.; deMello, A. J.; Kovalenko, M. V. Exploration of Near-Infrared-Emissive Colloidal Multinary Lead Halide Perovskite Nanocrystals Using an Automated Microfluidic Platform. *ACS Nano* **2018**, *12* (6), 5504−5517.
(32) Swarnkar, A.; Chulliyil, R.; Ravi, V. K.; Irfanullah, M.; Chowdhury, A.; Nag, A. Colloidal CsPbBr3 Perovskite Nanocrystals: Luminescence beyond Traditional Quantum Dots. *Angew. Chem., Int. Ed.* **2015**, *54* (51), 15424−15428.
(33) Tong, Y.; Bladt, E.; Ayguler, M. F.; Manzi, A.; Milowska, K. Z.; Hintermayr, V. A.; Docampo, P.; Bals, S.; Urban, A. S.; Polavarapu, L.; Feldmann, J. Highly Luminescent Cesium Lead Halide Perovskite Nanocrystals with Tunable Composition and Thickness by Ultrasonication. *Angew. Chem., Int. Ed.* **2016**, *55* (44), 13887−13892.
(34) Akkerman, Q. A.; Gandini, M.; Di Stasio, F.; Rastogi, P.; Palazon, F.; Bertoni, G.; Ball, J. M.; Prato, M.; Petrozza, A.; Manna, L. Strongly emissive perovskite nanocrystal inks for high-voltage solar cells. *Nat. Energy* **2017**, *2*, 16194.
(35) Dutta, A.; Pradhan, N. Phase-Stable Red-Emitting CsPbI3 Nanocrystals: Successes and Challenges. *ACS Energy Lett.* **2019**, *4* (3), 709−719.
(36) Dutta, A.; Dutta, S. K.; Das Adhikari, S.; Pradhan, N. Tuning the Size of CsPbBr3 Nanocrystals: All at One Constant Temperature. *ACS Energy Lett.* **2018**, *3* (2), 329−334.
(37) Krieg, F.; Ochsenbein, S. T.; Yakunin, S.; ten Brinck, S.; Aellen, P.; Süess, A.; Clerc, B.; Guggisberg, D.; Nazarenko, O.; Shynkarenko, Y.; Kumar, S.; Shih, C. J.; Infante, I.; Kovalenko, M. V. Colloidal CsPbX3 (X = CI, Br, I) Nanocrystals 2.0: Zwitterionic Capping Ligands for Improved Durability and Stability. *ACS Energy Lett.* **2018**, *3* (3), 641−646.
(38) Imran, M.; Caligiuri, V.; Wang, M. J.; Goldoni, L.; Prato, M.; Krahne, R.; De Trizio, L.; Manna, L. Benzoyl Halides as Alternative Precursors for the Colloidal Synthesis of Lead-Based Halide Perovskite Nanocrystals. *J. Am. Chem. Soc.* **2018**, *140* (7), 2656−2664.
(39) Weidman, M. C.; Seitz, M.; Stranks, S. D.; Tisdale, W. A. Highly Tunable Colloidal Perovskite Nanoplatelets through Variable Cation, Metal, and Halide Composition. *ACS Nano* **2016**, *10* (8), 7830−7839.
(40) Song, J. Z.; Li, J. H.; Xu, L. M.; Li, J. H.; Zhang, F. J.; Han, B. N.; Shan, Q. S.; Zeng, H. B. Room-Temperature Triple-Ligand Surface Engineering Synergistically Boosts Ink Stability, Recombination Dynamics, and Charge Injection toward EQE-11.6% Perovskite QLEDs. *Adv. Mater.* **2018**, *30* (30), 1800764.
(41) Levchuk, I.; Osvet, A.; Tang, X.; Brandl, M.; Perea, J. D. o.; Hoegl, F.; Matt, G. J.; Hock, R.; Batentschuk, M.; Brabec, C. J. Brightly Luminescent and Color-Tunable Formamidinium Lead Halide Perovskite FAPbX3 (X = Cl, Br, I) Colloidal Nanocrystals. *Nano Lett.* **2017**, *17* (5), 2765−2770.
(42) Zhang, D. D.; Eaton, S. W.; Yu, Y.; Dou, L. T.; Yang, P. D. Solution-Phase Synthesis of Cesium Lead Halide Perovskite Nanowires. *J. Am. Chem. Soc.* **2015**, *137* (29), 9230−9233.
(43) Bodnarchuk, M. I.; Boehme, S. C.; ten Brinck, S.; Bernasconi, C.; Shynkarenko, Y.; Krieg, F.; Widmer, R.; Aeschlimann, B.; Gunther, D.; Kovalenko, M. V.; Infante, I. Rationalizing and Controlling the Surface Structure and Electronic Passivation of Cesium Lead Halide Nanocrystals. *ACS Energy Lett.* **2019**, *4* (1), 63−74.
(44) Maceiczyk, R. M.; Dumbgen, K.; Lignos, I.; Protesescu, L.; Kovalenko, M. V.; deMello, A. J. Microfluidic Reactors Provide Preparative and Mechanistic Insights into the Synthesis of Formamidinium Lead Halide Perovskite Nanocrystals. *Chem. Mater.* **2017**, *29* (19), 8433−8439.
(45) Lignos, I.; Protesescu, L.; Emiroglu, D. B.; Maceiczyk, R.; Schneider, S.; Kovalenko, M. V.; deMello, A. J. Unveiling the Shape Evolution and Halide-Ion-Segregation in Blue-Emitting Formamidinium Lead Halide Perovskite Nanocrystals Using an Automated Microfluidic Platform. *Nano Lett.* **2018**, *18* (2), 1246−1252.
(46) Lignos, I.; Stavrakis, S.; Nedelcu, G.; Protesescu, L.; Demello, A. J.; Kovalenko, M. V. Synthesis of Cesium Lead Halide Perovskite Nanocrystals in a Droplet-Based Microfluidic Platform: Fast Parametric Space Mapping. *Nano Lett.* **2016**, *16* (3), 1869−1877.
(47) Udayabhaskararao, T.; Kazes, M.; Houben, L.; Lin, H.; Oron, D. Nucleation, Growth, and Structural Transformations of Perovskite Nanocrystals. *Chem. Mater.* **2017**, *29* (3), 1302−1308.
(48) De Roo, J.; Ibanez, M.; Geiregat, P.; Nedelcu, G.; Walravens, W.; Maes, J.; Martins, J. C.; Van Driessche, I.; Kovalenko, M. V.; Hens, Z. Highly Dynamic Ligand Binding and Light Absorption Coefficient of Cesium Lead Bromide Perovskite Nanocrystals. *ACS Nano* **2016**, *10* (2), 2071−2081.
(49) Guo, Y.; Shoyama, K.; Sato, W.; Nakamura, E. Polymer Stabilization of Lead(II) Perovskite Cubic Nanocrystals for Semitransparent Solar Cells. *Adv. Energy Mater.* **2016**, *6* (6), 1502317.
(50) Huang, H.; Chen, B.; Wang, Z.; Hung, T. F.; Susha, A. S.; Zhong, H.; Rogach, A. L. Water resistant CsPbX3 nanocrystals coated with polyhedral oligomeric silsesquioxane and their use as solid state

DOI: 10.1021/acs.chemmater.9b03438
Chem. Mater. 2020, 32, 27−37

luminophores in all-perovskite white light-emitting devices. *Chem. Sci.* **2016**, *7* (9), 5699−5703.
(51) Kim, Y.; Yassitepe, E.; Voznyy, O.; Comin, R.; Walters, G.; Gong, X.; Kanjanaboos, P.; Nogueira, A. F.; Sargent, E. H. Efficient Luminescence from Perovskite Quantum Dot Solids. *ACS Appl. Mater. Interfaces* **2015**, *7* (45), 25007−25013.
(52) Pan, J.; Sarmah, S. P.; Murali, B.; Dursun, I.; Peng, W.; Parida, M. R.; Liu, J.; Sinatra, L.; Alyami, N.; Zhao, C.; Alarousu, E.; Ng, T. K.; Ooi, B. S.; Bakr, O. M.; Mohammed, O. F. Air-Stable Surface-Passivated Perovskite Quantum Dots for Ultra-Robust, Single- and Two-Photon-Induced Amplified Spontaneous Emission. *J. Phys. Chem. Lett.* **2015**, *6* (24), 5027−5033.
(53) Grisorio, R.; Di Clemente, M. E.; Fanizza, E.; Allegretta, I.; Altamura, D.; Striccoli, M.; Terzano, R.; Giannini, C.; Irimia-Vladu, M.; Suranna, G. P. Exploring the surface chemistry of cesium lead halide perovskite nanocrystals. *Nanoscale* **2019**, *11* (3), 986−999.
(54) Makarov, N. S.; Guo, S.; Isaienko, O.; Liu, W.; Robel, I.; Klimov, V. I. Spectral and Dynamical Properties of Single Excitons, Biexcitons, and Trions in Cesium-Lead-Halide Perovskite Quantum Dots. *Nano Lett.* **2016**, *16* (4), 2349−2362.
(55) Park, Y.-S.; Guo, S.; Makarov, N. S.; Klimov, V. I. Room Temperature Single-Photon Emission from Individual Perovskite Quantum Dots. *ACS Nano* **2015**, *9* (10), 10386−10393.
(56) Raino, G.; Nedelcu, G.; Protesescu, L.; Bodnarchuk, M. I.; Kovalenko, M. V.; Mahrt, R. F.; Stoeferle, T. Single Cesium Lead Halide Perovskite Nanocrystals at Low Temperature: Fast Single Photon Emission, Reduced Blinking, and Exciton Fine Structure. *ACS Nano* **2016**, *10* (2), 2485−2490.
(57) Tian, Y.; Merdasa, A.; Peter, M.; Abdellah, M.; Zheng, K.; Ponseca, C. S., Jr.; Pullerits, T.; Yartsev, A.; Sundstrom, V.; Scheblykin, I. G. Giant Photoluminescence Blinking of Perovskite Nanocrystals Reveals Single-Trap Control of Luminescence. *Nano Lett.* **2015**, *15* (3), 1603−1608.
(58) Utzat, H.; Shulenberger, K. E.; Achorn, O. B.; Nasilowski, M.; Sinclair, T. S.; Bawendi, M. G. Probing Linewidths and Biexciton Quantum Yields of Single Cesium Lead Halide Nanocrystals in Solution. *Nano Lett.* **2017**, *17* (11), 6838−6846.
(59) Becker, M. A.; Vaxenburg, R.; Nedelcu, G.; Sercel, P. C.; Shabaev, A.; Mehl, M. J.; Michopoulos, J. G.; Lambrakos, S. G.; Bernstein, N.; Lyons, J. L.; Stoferle, T.; Mahrt, R. F.; Kovalenko, M. V.; Norris, D. J.; Raino, G.; Efros, A. L. Bright triplet excitons in caesium lead halide perovskites. *Nature* **2018**, *553* (7687), 189−193.
(60) Utzat, H.; Sun, W. W.; Kaplan, A. E. K.; Krieg, F.; Ginterseder, M.; Spokoyny, B.; Klein, N. D.; Shulenberger, K. E.; Perkinson, C. F.; Kovalenko, M. V.; Bawendi, M. G. Coherent single-photon emission from colloidal lead halide perovskite quantum dots. *Science* **2019**, *363* (6431), 1068−1072.
(61) Zhou, Y.; Zhao, Y. Chemical stability and instability of inorganic halide perovskites. *Energy Environ. Sci.* **2019**, *12* (5), 1495−1511.
(62) Zhou, Q.; Bai, Z.; Lu, W. G.; Wang, Y.; Zou, B.; Zhong, H. In Situ Fabrication of Halide Perovskite Nanocrystal-Embedded Polymer Composite Films with Enhanced Photoluminescence for Display Backlights. *Adv. Mater.* **2016**, *28* (41), 9163−9168.
(63) Lin, K.; Xing, J.; Quan, L. N.; de Arquer, F. P. G.; Gong, X.; Lu, J.; Xie, L.; Zhao, W.; Zhang, D.; Yan, C.; Li, W.; Liu, X.; Lu, Y.; Kirman, J.; Sargent, E. H.; Xiong, Q.; Wei, Z. Perovskite light-emitting diodes with external quantum efficiency exceeding 20%. *Nature* **2018**, *562* (7726), 245−248.
(64) Lin, X.; Dai, X. L.; Pu, C. D.; Deng, Y. Z.; Niu, Y.; Tong, L. M.; Fang, W.; Jin, Y. Z.; Peng, X. G. Electrically-driven single-photon sources based on colloidal quantum dots with near-optimal antibunching at room temperature. *Nat. Commun.* **2017**, *8*, 1132.
(65) Aharonovich, I.; Englund, D.; Toth, M. Solid-state single-photon emitters. *Nat. Photonics* **2016**, *10* (10), 631−641.
(66) Sercel, P. C.; Lyons, J. L.; Wickramaratne, D.; Vaxenburg, R.; Bernstein, N.; Efros, A. L. Exciton Fine Structure in Perovskite Nanocrystals. *Nano Lett.* **2019**, *19* (6), 4068−4077.
(67) Maceiczyk, R. M.; Lignos, I. G.; deMello, A. J. Online detection and automation methods in microfluidic nanomaterial synthesis. *Curr. Opin. Chem. Eng.* **2015**, *8*, 29−35.
(68) Lignos, I.; Maceiczyk, R.; deMello, A. J. Microfluidic Technology: Uncovering the Mechanisms of Nanocrystal Nucleation and Growth. *Acc. Chem. Res.* **2017**, *50* (5), 1248−1257.
(69) Phillips, T. W.; Lignos, I. G.; Maceiczyk, R. M.; deMello, A. J.; deMello, J. C. Nanocrystal synthesis in microfluidic reactors: where next? *Lab Chip* **2014**, *14* (17), 3172−3180.
(70) Locardi, F.; Cirignano, M.; Baranov, D.; Dang, Z.; Prato, M.; Drago, F.; Ferretti, M.; Pinchetti, V.; Fanciulli, M.; Brovelli, S.; De Trizio, L.; Manna, L. Colloidal Synthesis of Double Perovskite Cs2AgInCl6 and Mn-Doped Cs2AgInCl6 Nanocrystals. *J. Am. Chem. Soc.* **2018**, *140* (40), 12989−12995.
(71) Locardi, F.; Sartori, E.; Buha, J.; Zito, J.; Prato, M.; Pinchetti, V.; Zaffalon, M. L.; Ferretti, M.; Brovelli, S.; Infante, I.; De Trizio, L.; Manna, L. Emissive Bi-Doped Double Perovskite Cs2Ag1−xNaxInCl6 Nanocrystals. *ACS Energy Lett.* **2019**, *4*, 1976−1982.
(72) Yang, B.; Mao, X.; Hong, F.; Meng, W.; Tang, Y.; Xia, X.; Yang, S.; Deng, W.; Han, K. Lead-Free Direct Band Gap Double-Perovskite Nanocrystals with Bright Dual-Color Emission. *J. Am. Chem. Soc.* **2018**, *140* (49), 17001−17006.
(73) Yang, B.; Chen, J.; Yang, S.; Hong, F.; Sun, L.; Han, P.; Pullerits, T.; Deng, W.; Han, K. Lead-Free Silver-Bismuth Halide Double Perovskite Nanocrystals. *Angew. Chem., Int. Ed.* **2018**, *57* (19), 5359−5363.
(74) Abecassis, B.; Bouet, C.; Garnero, C.; Constantin, D.; Lequeux, N.; Ithurria, S.; Dubertret, B.; Pauw, B. R.; Pontoni, D. Real-Time in Situ Probing of High-Temperature Quantum Dots Solution Synthesis. *Nano Lett.* **2015**, *15* (4), 2620−2626.
(75) Abolhasani, M.; Coley, C. W.; Xie, L. S.; Chen, O.; Bawendi, M. G.; Jensen, K. F. Oscillatory Microprocessor for Growth and in Situ Characterization of Semiconductor Nanocrystals. *Chem. Mater.* **2015**, *27* (17), 6131−6138.
(76) Lignos, I.; Protesescu, L.; Stavrakis, S.; Piveteau, L.; Speirs, M. J.; Loi, M. A.; Kovalenko, M. V.; deMello, A. J. Facile Droplet-based Microfluidic Synthesis of Monodisperse IV-VI Semiconductor Nanocrystals with Coupled In-Line NIR Fluorescence Detection. *Chem. Mater.* **2014**, *26* (9), 2975−2982.
(77) Maceiczyk, R. M.; Bezinge, L.; deMello, A. J. Kinetics of nanocrystal synthesis in a microfluidic reactor: theory and experiment. *React. Chem. Eng.* **2016**, *1*, 261−271.
(78) Nightingale, A. M.; Krishnadasan, S. H.; Berhanu, D.; Niu, X.; Drury, C.; McIntyre, R.; Valsami-Jones, E.; deMello, J. C. A stable droplet reactor for high temperature nanocrystal synthesis. *Lab Chip* **2011**, *11* (7), 1221−1227.
(79) Schiener, A.; Magerl, A.; Krach, A.; Seifert, S.; Steinruck, H. G.; Zagorac, J.; Zahn, D.; Weihrich, R. In situ investigation of two-step nucleation and growth of CdS nanoparticles from solution. *Nanoscale* **2015**, *7* (26), 11328−11333.
(80) Xie, L.; Shen, Y.; Franke, D.; Sebastian, V.; Bawendi, M. G.; Jensen, K. F. Characterization of Indium Phosphide Quantum Dot Growth Intermediates Using MALDI-TOF Mass Spectrometry. *J. Am. Chem. Soc.* **2016**, *138* (41), 13469−13472.
(81) Abdel-Latif, K.; Epps, R. W.; Kerr, C. B.; Papa, C. M.; Castellano, F. N.; Abolhasani, M. Facile Room-Temperature Anion Exchange Reactions of Inorganic Perovskite Quantum Dots Enabled by a Modular Microfluidic Platform. *Adv. Funct. Mater.* **2019**, *29* (23), 1900712.
(82) Baek, J.; Shen, Y.; Lignos, I.; Bawendi, M. G.; Jensen, K. F. Multistage Microfluidic Platform for the Continuous Synthesis of III-V Core/Shell Quantum Dots. *Angew. Chem., Int. Ed.* **2018**, *57* (34), 10915−10918.
(83) Bezinge, L.; Maceiczyk, R. M.; Lignos, I.; Kovalenko, M. V.; Demello, A. J. Pick a Color MARIA: Adaptive Sampling Enables the Rapid Identification of Complex Perovskite Nanocrystal Compositions with Defined Emission Characteristics. *ACS Appl. Mater. Interfaces* **2018**, *10* (22), 18869−18878.

DOI: 10.1021/acs.chemmater.9b03438
Chem. Mater. 2020, 32, 27−37

(84) Epps, R. W.; Felton, K. C.; Coley, C. W.; Abolhasani, M. Automated microfluidic platform for systematic studies of colloidal perovskite nanocrystals: towards continuous nano-manufacturing. *Lab Chip* **2017**, *17* (23), 4040−4047.
(85) Guidelli, E. J.; Lignos, I.; Yoo, J. J.; Lusardi, M.; Bawendi, M. G.; Baffa, O.; Jensen, K. F. Mechanistic Insights and Controlled Synthesis of Radioluminescent ZnSe Quantum Dots Using a Microfluidic Reactor. *Chem. Mater.* **2018**, *30* (23), 8562−8570.
(86) Li, C.; Ding, B.; Zhang, L.; Song, K.; Tao, S. 3D-printed continuous flow reactor for high yield synthesis of CH3NH3PbX3 (X = Br, I) nanocrystals. *J. Mater. Chem. C* **2019**, *7*, 9167−9174.
(87) Lignos, I.; Stavrakis, S.; Kilaj, A.; deMello, A. J. Millisecond-Timescale Monitoring of PbS Nanoparticle Nucleation and Growth Using Droplet-Based Microfluidics. *Small* **2015**, *11* (32), 4009−4017.
(88) Polte, J.; Erler, R.; Thünemann, A. F.; Sokolov, S.; Ahner, T. T.; Rademann, K.; Emmerling, F.; Kraehnert, R. Nucleation and growth of gold nanoparticles studied via in situ small angle X-ray scattering at millisecond time resolution. *ACS Nano* **2010**, *4* (2), 1076−1082.
(89) Kuyper, C. L.; Budzinski, K. L.; Lorenz, R. M.; Chiu, D. T. Real-time sizing of nanoparticles in microfluidic channels using confocal correlation spectroscopy. *J. Am. Chem. Soc.* **2006**, *128* (3), 730−731.
(90) Qin, D.; Xia, Y.; Whitesides, G. M. Soft lithography for micro- and nanoscale patterning. *Nat. Protoc.* **2010**, *5* (3), 491−502.
(91) Chirvony, V. S.; González-Carrero, S.; Suárez, I.; Galian, R. E.; Sessolo, M.; Bolink, H. J.; Martínez-Pastor, J. P.; Pérez-Prieto, J. Delayed Luminescence in Lead Halide Perovskite Nanocrystals. *J. Phys. Chem. C* **2017**, *121* (24), 13381−13390.
(92) Rabouw, F. T.; Kamp, M.; van Dijk-Moes, R. J. A.; Gamelin, D. R.; Koenderink, A. F.; Meijerink, A.; Vanmaekelbergh, D. Delayed Exciton Emission and Its Relation to Blinking in CdSe Quantum Dots. *Nano Lett.* **2015**, *15* (11), 7718−7725.
(93) Rabouw, F. T.; van der Bok, J. C.; Spinicelli, P.; Mahler, B.; Nasilowski, M.; Pedetti, S.; Dubertret, B.; Vanmaekelbergh, D. Temporary Charge Carrier Separation Dominates the Photoluminescence Decay Dynamics of Colloidal CdSe Nanoplatelets. *Nano Lett.* **2016**, *16* (3), 2047−2053.
(94) Pope, M.; Swenberg, C. E.; Pope, M. *Electronic processes in organic crystals and polymers*, 2nd ed.; Oxford University Press: New York, 1999.

DOI: 10.1021/acs.chemmater.9b03438
Chem. Mater. 2020, 32, 27−37